USGS
science for a changing world

Modeling Wave and Seabed Energetics on the California Continental Shelf

By Li H. Erikson, Curt D. Storlazzi, and Nadine E. Golden

Suggested citation:

Erikson, Li H., Storlazzi, Curt D., and Golden, Nadine E., 2014. Modeling Wave and Seabed Energetics on the California Continental Shelf. U. S. Geological Survey summary of methods to accompany data set, doi:10.5066/F7125QNQ.

2014

U.S. Department of the Interior
U.S. Geological Survey

Contents

Figures

Tables

Conversion Factors

SI to Inch/Pound

Multiply	By	To obtain
	Length	
centimeter (cm)	0.3937	inch (in)
millimeter (mm)	0.03937	inch (in)
meter (m)	3.281	foot (ft)
kilometer (km)	0.6214	mile (mi)
kilometer (km)	0.5400	mile, nautical (nmi)
meter (m)	1.094	yard (yd)

Modeling Wave and Seabed Energetics on the California Continental Shelf

By Li H. Erikson, Curt D. Storlazzi, and Nadine E. Golden

Chapter 1. Introduction

Background and motivation

Ecologists have long recognized that the structure and function of benthic marine ecosystems are closely linked to oceanographic processes (Mann, 1973; Graham and others, 1997; Snelgrove and Butman, 1994); most studies, however, have relied either upon qualitative descriptions of oceanographic factors (such as, “low”, “medium”, or “high” energy environments) or on quantitative values based on mean oceanographic conditions (e.g., tidal range or wave heights). Recently, the importance of intermittent disturbance on marine habitats has been addressed by Thrush and Dayton (2002), Roff and others (2003), and Goodsell and Connell (2005) among others. These studies show that quantifying the natural spatial and temporal variability of disturbances affecting benthic marine ecosystems can be critical for managers and planners tasked with forecasting the effects of particular management practices such as marine protected areas. Understanding the natural variability of sea floor disturbance is also critical for local, State, and Federal agencies responsible for permitting offshore activities such as trawling, dredging, and the placement of sea-floor engineering structures (such as cables and pipelines) that disturb the sea floor.

The oceanographic processes that disturb the continental shelf include the actions of surface waves, internal waves, and currents (tidal, density, wave-driven, wind-driven, and geostrophic). The North Pacific Ocean can generate extremely large surface waves, and the resulting near-bed wave orbital velocities on the continental shelf generally are much larger than velocities due to currents and internal waves (Sherwood and others, 1994; Storlazzi and Jaffe, 2002; Storlazzi and others, 2003). Although many studies have investigated the wave climate along central California (such as Inman and Jenkins, 1997; Allan and Komar, 2000; Bromirski and others, 2005) and the influence of the El Niño-Southern Oscillation (ENSO) on those waves (Seymour and others, 1984; Seymour, 1998; Storlazzi and Griggs, 2000), none have investigated how spatial and temporal variations in wave climate influence sediment mobility on the California continental shelf. On the other hand, while Porter-Smith and others (2004), Hemer (2006), and Griffen and others (2008) investigated the impact of waves on the Australian continental shelf, they did not address how these patterns would change through time due to variations in meteorologic and oceanographic forcing. It thus appears that although our understanding of the processes controlling sea floor dynamics on continental shelf scales has improved over the past decade, our ability to predict them over large spatial and temporal scales remains limited. Varying wave climates can not only impact sea-floor processes, but also benthic and pelagic ecosystems that rely on them and influence their recovery from anthropogenically-induced perturbations.

Recently, Storlazzi and Reid (2010) investigated the impact of waves along the central California (Bodega Head to Point Sur) continental margin under the influence of ENSO cycles. Spatial maps of wave conditions were modeled numerically using the SWAN model (Ris, 1997; Booij and others, 1999; Ris and others, 1999) and boundary forcing derived from monthly statistics of more than 14 years of concurrent hourly oceanographic and meteorological data from a NOAA buoy (National Data Buoy Center, 2006). Wave growth and propagation were modeled in order to understand how

variations in wave forcing results impacts to the sea floor spatially and temporally. In this study, the work of Storlazzi and Reid (2010) is spatially extended to encompass the entire California coast. Additionally, this study focuses on seasonal means and extremes rather than ENSO cycles and relies on 32 years (1984 to 2011) of hourly hind-cast data, compared to 14 years of in situ buoy measurements in the earlier study.

Publication Summary

This publication concerns model-derived wave and seabed energetics across the inner margin of the California continental shelf and includes 1800 downloadable geographic information (GIS) files (600 for wave heights, wave periods, and orbital velocities, each). The downloadable files consist of two-dimensional spatial maps of near-bed wave-orbital velocities and significant wave heights, peak wave periods, and peak wave directions for representative mean and extreme conditions during winter, spring, summer, and fall. The remainder of this document describes the model and data used to derive the spatial maps, compares model data with available observations, and provides a brief overview of the results. No detailed discussion of results and its applications are provided herein.

Chapter 2. Methods

Wave Modeling

Patterns of wave energy and orbital velocities along the California coast were simulated with the numerical wave model SWAN (Simulating Waves Nearshore, Delft University of Technology, The Netherlands). SWAN is a third-generation spectral wave model capable of simulating wind-wave growth, propagation, refraction, dissipation, and depth-induced breaking (Booij and others 1999; Ris, 1997). Since its initial release in 1998, the model has become a widely used tool for offshore and nearshore wave calculations.

A set of 15 SWAN model grids were developed and used to simulate wind-wave growth and propagation across the inner portion of the California continental shelf (fig. 1). All grids were curvi-linear, with an average cross- and along-shore resolution of 30 to 50 m and 60 to 100 m, respectively, in the shallow inshore regions. Model grid cells were smaller in the cross-shore direction, in shallow water, and around complex bathymetry to enable accurate wave refraction and shoaling. Latitudinal extents were defined based on local geography and computation limitations. The offshore extent of the model grids were defined by 64 Wave Information System (WIS, *http://wis.usace.army.mil/*) model output stations located approximately 20 km offshore along the entire California coast (Table 1). WIS data are discussed further in the next section. Wave parameters (significant wave heights, peak wave period, and mean wave direction) derived from the WIS database were applied at the boundaries of the 15 SWAN grids (fig. 1). Parametric wave descriptors (wave heights, periods, and wave direction) derived from the WIS database were applied along the open boundaries of the SWAN domains; these were represented in spectral space with a JONSWAP shape and a 3.3 peak enhancement factor. In all grids, 10-degree direction bins and 36 frequencies spaced log-normally from 0.0417 Hz to 1.0000 Hz were used. The bottom friction coefficient was set to $0.038 m^2/s$ for swell conditions (Hasselmann and others, 1973 in SWAN technical documentation, 2013), whitecapping was computed with the Komen and others (1984) formulation, and depth induced breaking with the Battjes and Janssen (1978) formulation. Winds from the most centrally located WIS station of each grid were applied uniformly across the domains to allow for inclusion of locally wind-generated waves in addition to (usually greater) energy contributions from distantly generated swell waves. All grids were solved in the spherical coordinate system and run in a stationary mode.

Table 1. Grids employed in the wave model and associated WIS open boundary stations and latitudinal extents.

SWAN grid	WIS station IDs	Approximate north-south extents
ca1	83039 to 83045	Oregon border to Trinidad
ca2	83046 to 83049	Trinidad to Ferndale
ca3	83050 to 83052	Ferndale to Shelter Cove
ca4	83053 to 83056	Shelter Cove to Fort Bragg
ca5	83056 to 83059	Fort Bragg to Point Arena
ca6	83059 to 83062	Point Arena to Jenner
ca7	83062 to 83066	Jenner to Daly City
ca8	83066 to 83070	Daly City to Pescadero
ca9	83070 to 83075	Pescadero to north Big Sur coast
ca10	83075 to 83078	North Big Sur coast to Lucia
ca11	83078 to 83081	Lucia to Morro Bay
ca12	83082 to 83089	Morro Bay to Vandenberg Air Force Base
ca13	83086 to 83093; 83096	Vandenberg to Oxnard
ca14	83096; 83099 to 83103; 83105	Oxnard to Oceanside
ca15	83104 to 83105; 83107	San Clemente to Mexican border

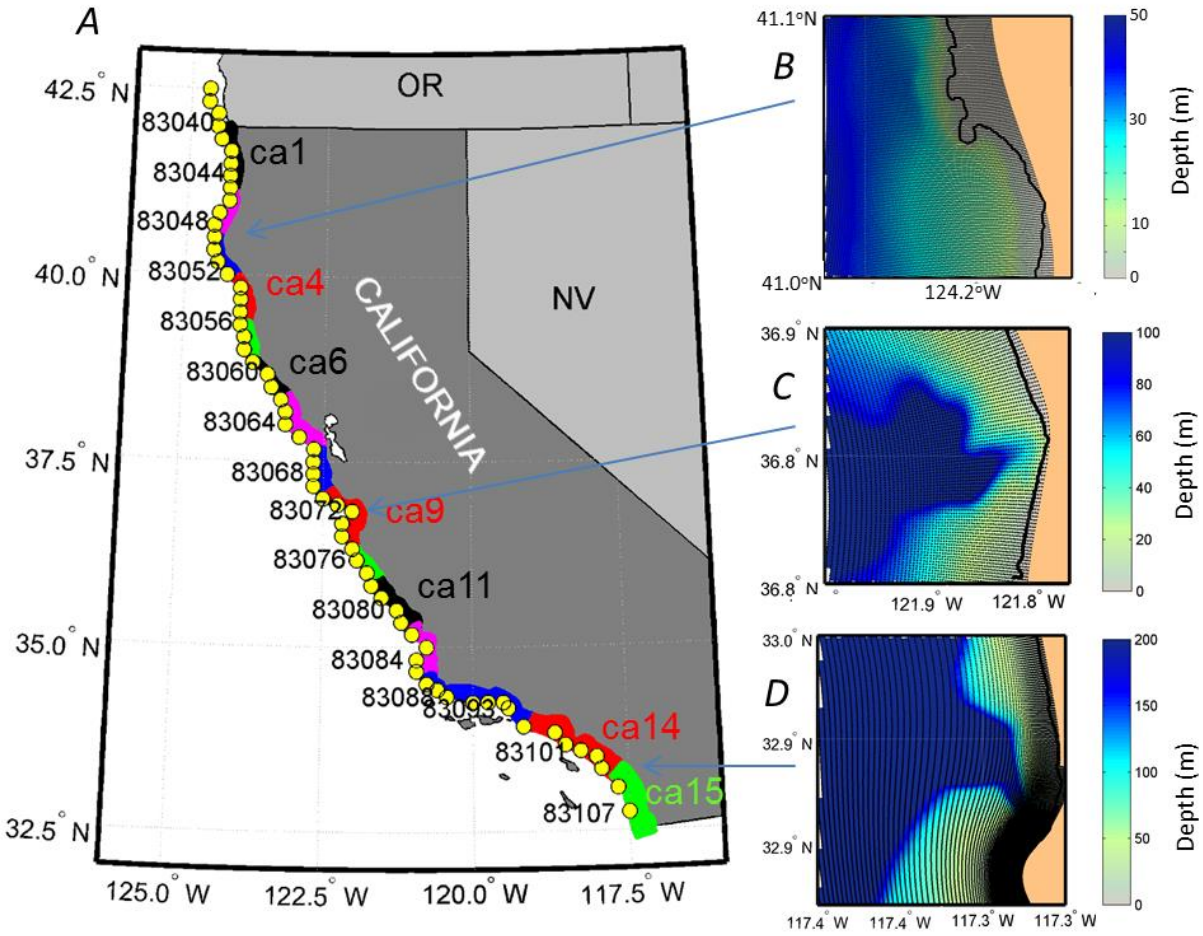

Figure 1. Map of the study area and examples of the model domains.

(*A*) Map of 15 SWAN grids along the California coast used in the study. Yellow dots denote the location of WIS boundary points used in the model simulations; station IDs are shown for every fourth boundary point. Example close-up views of the grids and bathymetry in the vicinity of (*B*) Trinidad, (*C*) Monterey Canyon, and (*D*) La Jolla Canyon display the great bathymetric and topographic variability that results in large spatial gradients of wave energy along California.

In shallow water, the orbital motions of water particles induced by surface waves extend down to the seabed (see inset). The resulting wave-induced orbital velocities near the seabed are considered to be a representative measure of how waves influence the sea floor and as such are a focus of this study. The SWAN model calculates bottom orbital velocity (U_{orb}) as the maxima of the root mean square (rms) bottom velocity (U_{rms}):

$$U_{rms}^2 = \int_0^{2\pi} \int_0^{\infty} \frac{\delta^2}{sinh^2(kd)} E(\delta,\theta) d_\delta d_\theta \quad (1)$$

where δ is the wave frequency; θ is the wave direction; k is the wave number ($= 2\pi/L$) with L as the wavelength which in turn is related to the constant π, acceleration due to gravity (g = 9.81 m/s^2), water depth d, and wave period , T; and E(δ,θ) is the wave energy density related to g, δ, θ, water density, and wave height (H). In essence, the orbital velocities are a function of three primary wave descriptors, namely the wave height, wave period, and wavelength.

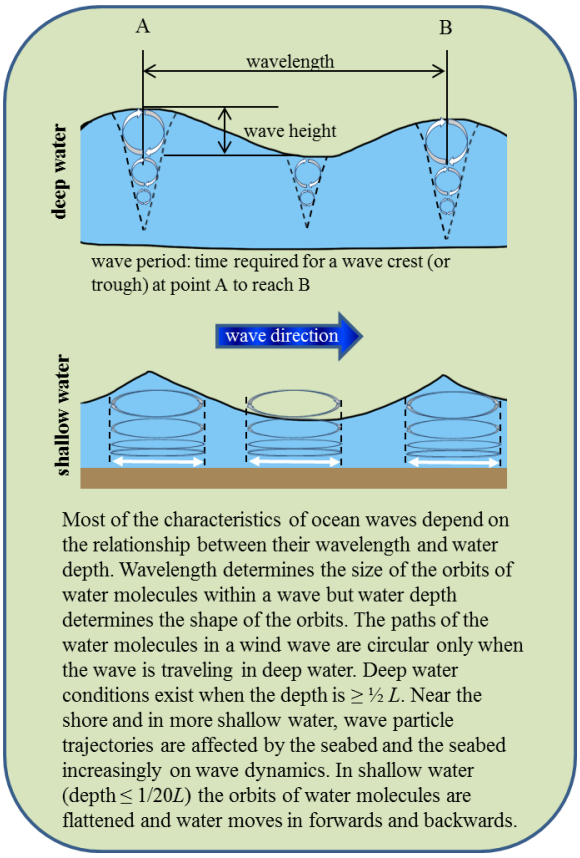

Wave energy flux is the rate at which energy is transmitted in the direction of wave propagation across a vertical plane perpendicular to the direction of wave advance and extending throughout the water column (Demirbilik and Linwood, 2002). Assuming linear wave theory, the average energy flux per unit wave crest transmitted across a vertical plane and perpendicular to the direction of wave advance, also known as wave power $\bar{P}$, may be expressed as

$$\bar{P} = \bar{E} C_g \quad (2)$$

where $\bar{E}$ is the specific energy density $=1/8\,\rho g H^2$, and C_g the group velocity which depends on relative water depth

$$C_g = \sqrt{gd} \quad \text{for shallow water, } d/L<1/20 \quad (3)$$

$$C_g = nC = \frac{1}{2}\left[1 + \frac{4\pi d/L}{\sinh(4\pi d/L)}\right] C, C = L/T \quad \text{for transitional water, } 1/20 < d/L < 1/2 \quad (4)$$

$$C_g = \frac{gT}{4\pi} \quad \text{for deep water, } d/L>1/2 \quad (5)$$

Estimates of total $\bar{P}$ for all wave directions were calculated for each of the model domains, each season, and statistic (mean and top 5%). These data are not directly provided in downloadable files but can be computed with the relationships listed above.

Wave and wind data employed at model boundaries

Wave and wind data used as boundary conditions to the models run as part of this study were obtained from the Coastal and Hydraulics Laboratory (2013) Wave Information System (WIS) study. In that study, wave hind-casts were calculated with the numerical wave model WAM (Wave Prediction Model) Cycle 4.5.1C (Gunther and others, 1992; Komen and others, 1994) on a 0.25° grid (approximately 28 km at 37°N). Ten-meter height neutrally stable marine winds, compiled and analyzed by Oceanweather, Inc. (2012), were used as boundary conditions in the WAM model. It is worth noting that the basic scientific philosophy of SWAN and WAM are the same. The models use similar formulations for the source terms and both describe wave generation and evolution of the wave spectrum by solving the action balance equation. The main difference between the models is the

numerical implementation and inclusion of additional nearshore processes (depth-induced breaking and triad wave-wave interactions) in the SWAN model.

Continuous hourly wave and wind parameter time-series provided by the WIS study and encompassing the 32 years from 1980 through 2011 were used to calculate seasonal (arithmetic) mean and extreme (arithmetic mean of highest 5%) conditions. Seasons were defined as: winter = December through February; spring = March through May; summer = June through August; and fall = September through November.

Chapter 3. Model calibration and validation

The ability of the model to accurately simulate wave propagation was tested by running the model forced with hourly wave parameters of the WIS database over a week long time period from 18-25 January 2010. The simulation period encompasses a large storm event when wave heights exceeded 9 m (e.g., CDIP Pt. Reyes buoy) and affected the entire California coast.

The ability of the model to reproduce observed wave conditions was evaluated with a skill score, where (Willmott 1981):

$$skill = 1 - \frac{\sum_{i=1}^{N} |X_{mod} - X_{obs}|^2}{\sum_{i=1}^{N} [|X_{mod} - \bar{X}_{obs}| + |X_{obs} - \bar{X}_{obs}|]^2} \quad (6)$$

where X is H , and the subscripts *obs* and *mod* indicate measured and modeled values, respectively. Over-bars indicate time-averaged values. The skill score ranges from 0 to 1, with a skill score of 1 indicating perfect agreement. The analysis is done over the entire simulated time-series.

Skill scores are quite good (>0.80, Table 2) at all sites evaluated. The mean values and standard deviations are also within reason of each other. While observations are not available within all grids, the high skill scores and lack of clear geographic trend in changes of the skill score suggest that model results in grids with no buoys are likely also reflective of true conditions.

Table 2. Skill scores and mean value statistics of modeled and observed significant wave heights. Comparison is for 18-25 January 2010. Mean values and standard deviations (shown in parenthesis) are rounded to the nearest 0.05m.

NDBC ID	Owner/ operator	Longitude (°W)	Latitude (°N)	Model grid	Skill	Model mean & std	Observed mean & std
46027	NDBC	124.381	41.850	ca1	0.91	3.50 (1.20)	3.65 (1.25)
46237	SCRIPPS	122.599	37.781	ca7	0.91	2.65 (1.10)	3.20 (1.50)
46240	SCRIPPS	121.907	36.626	ca9	0.92	1.25 (0.60)	1.45 (0.60)
46236	SCRIPPS	121.947	36.761	ca9	0.97	2.90 (1.35)	2.90 (1.20)
46215	SCRIPPS	120.860	35.204	ca12	0.97	2.60 (1.30)	2.65 (1.10)
46223	SCRIPPS	117.767	33.458	ca14	0.92	1.40 (0.90)	1.70 (0.90)
46222	SCRIPPS	118.317	33.618	ca14	0.84	1.45 (1.00)	2.00 (0.93)
46221	SCRIPPS	118.633	33.854	ca14	0.85	1.30 (0.95)	1.90 (0.85)
46231	SCRIPPS	117.370	32.748	ca15	0.81	1.40 (0.65)	2.00 (0.85)
46225	SCRIPPS	117.393	32.930	ca15	0.87	1.30 (0.65)	1.70 (0.80)
46241	SCRIPPS	117.292	33.003	ca15	0.86	1.15 (0.60)	1.50 (0.61)
46224	SCRIPPS	117.471	33.179	ca15	0.86	1.05 (0.50)	1.45 (0.80)
46242	SCRIPPS	117.440	33.220	ca15	0.90	1.00 (0.50)	1.25 (0.80)

NDBC: National Data Buoy Center
SCRIPPS: Scripps Institute of Oceanography, Coastal Data Information Program

Chapter 4. Summary of wave and seabed energetics

Wave heights and incident wave energy at the model boundaries

Mean and top 5% incident wave directions are all from the west to northwest along the open boundaries of the model grids (fig. 2). Mean incident wave directions range from 212º to 288º, whereas under extreme conditions of the top 5%, wave directions are more northerly ranging from 252º to 328º. The seasonal variation in mean incident wave directions is much smaller than those of extreme conditions: overall mean conditions vary by ±3º compared to ±11º for the averaged seasonal extreme directions. In northern California, summer extreme events originate from more northerly directions

compared to storms during the remaining times of the year. In southern California south of Point Conception, incident storm waves are from nearly identical directions independent of the season (fig. 2B).

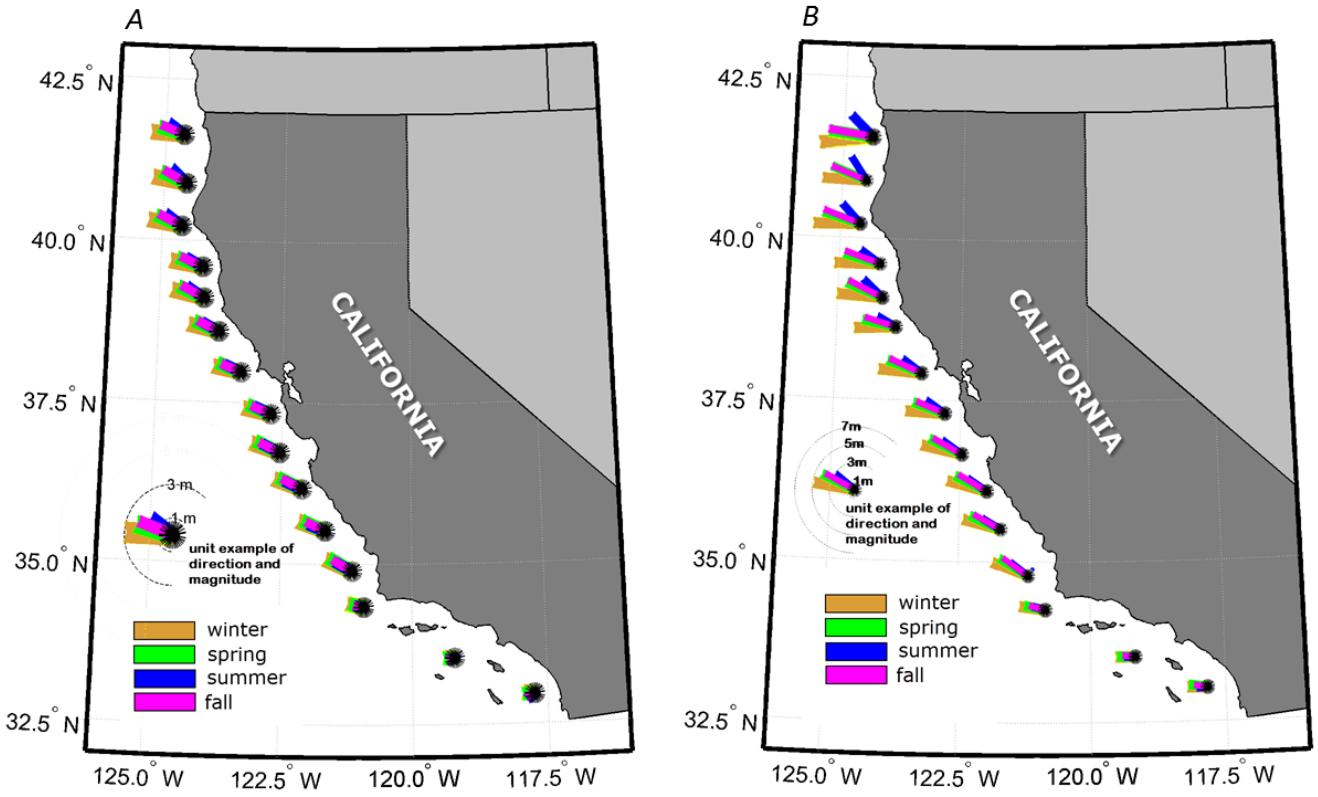

Figure 2. Seasonal wave heights and directions at model grid open boundaries. (*A*) Mean and (*B*) extreme (top 5%) wave heights and associated directions for the WIS station located at the approximate mid-point of each grid are shown.

Significant wave heights are smallest in summer and largest in winter, as expected. Mean summer conditions along the entire coast are 1.5 m ± 0.4 m whilst winter mean conditions are one meter higher with an average of 2.4 m ± 0.8 m. Seasonally averaged wave heights are greatest in northern California and smallest in Southern California (e.g., 3.3 m in north and less than 1.0 m in south during

the winter season). A similar pattern exists for extreme conditions. Winter extremes are on average 6.3 m in the north and 2.0 m in the south. Similarly, averaged extreme summer wave heights decrease from 3.2 m in the north to just over 1 m in the south. Spring and fall conditions also show a decreasing trend with decreasing latitude and both experience significant wave heights on the order of 5.0 m in the north. Whereas the deceasing trend is consistent, spring significant wave heights are typically greater than fall significant wave heights along the central and southern portions of the State.

Seasonally averaged peak wave periods (not shown but listed in Table A1) are longest in winter (15 s ± 1 s) and shortest in summer (10 s ± 3 s). The difference between wave periods of extreme conditions and background mean conditions is less than 2 s for all seasons.

Wave power and near-bed wave-orbital velocities

Wave power, simulated with the SWAN model, shows substantial variation along the California coast and across the continental shelf. Similar to forcing conditions at the model boundaries (previous section), wave power (eq. 2) is greatest in the north part of the State and smallest in the south (shaded colors in figs. 3 through 6). Winter and fall seasons (figs. 3 and 6) show the greatest difference between average ‘background’ and extreme conditions when wave power is as much as 5 times greater.

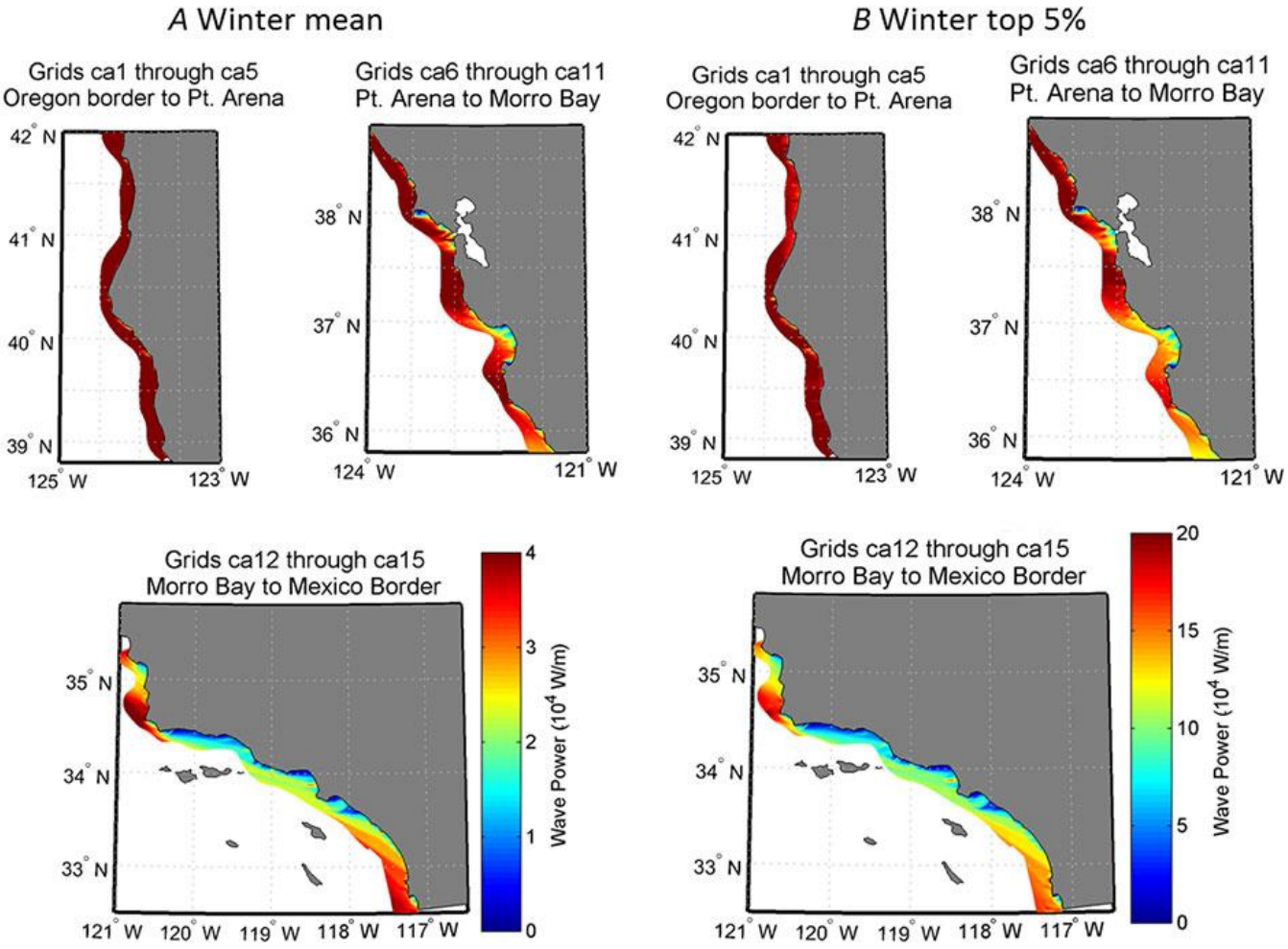

Figure 3. Winter (December-February) wave power along the inner margin of the California shelf. (*A*) Mean and (B) extreme (top 5%) conditions.

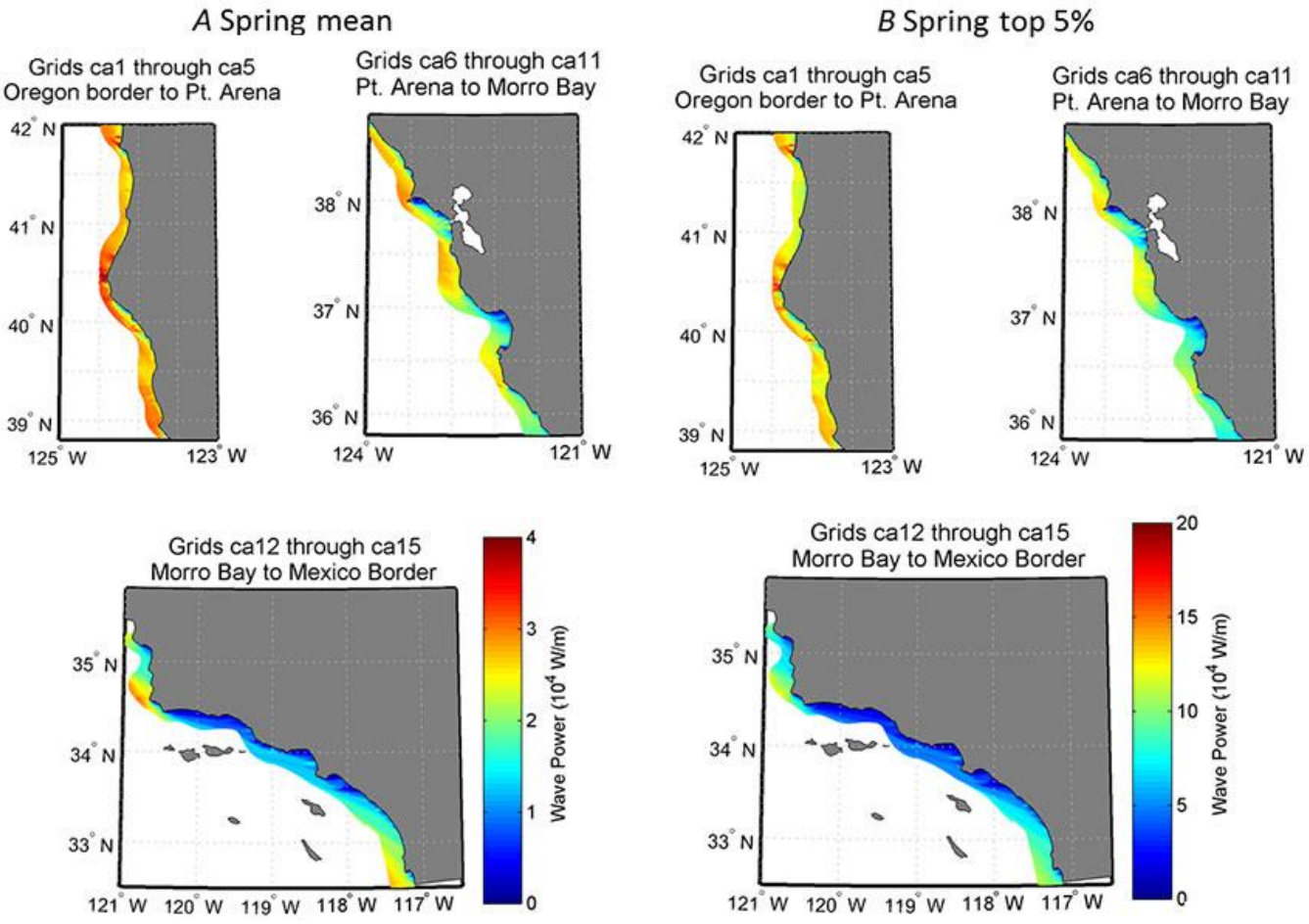

Figure 4. Spring (March-May) wave power along the inner margin of the California shelf. (*A*) Mean and (B) extreme (top 5%) conditions.

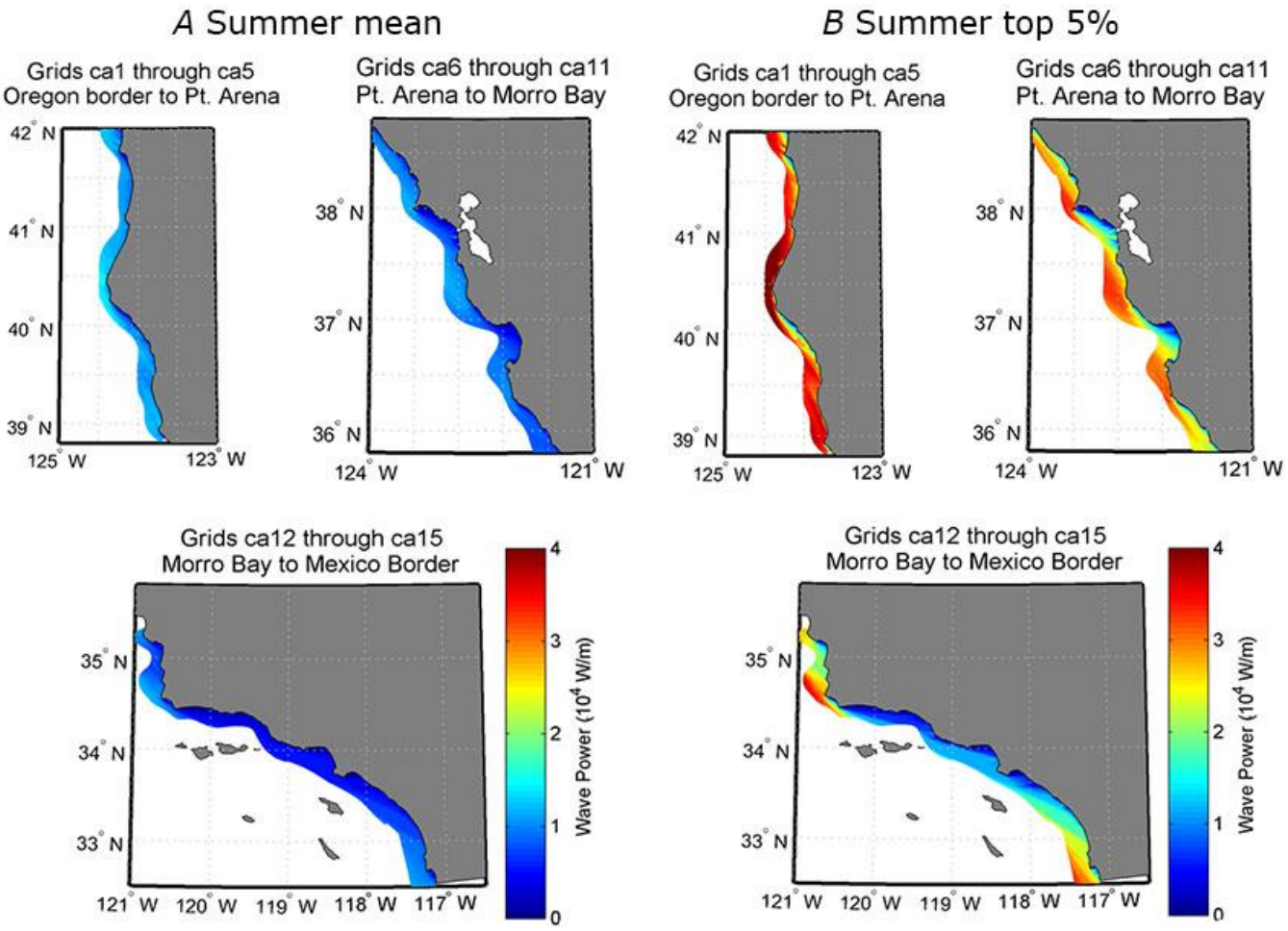

Figure 5. Summer (June-August) wave power along the inner margin of the California shelf. (*A*) Mean and (B) extreme (top 5%) conditions.

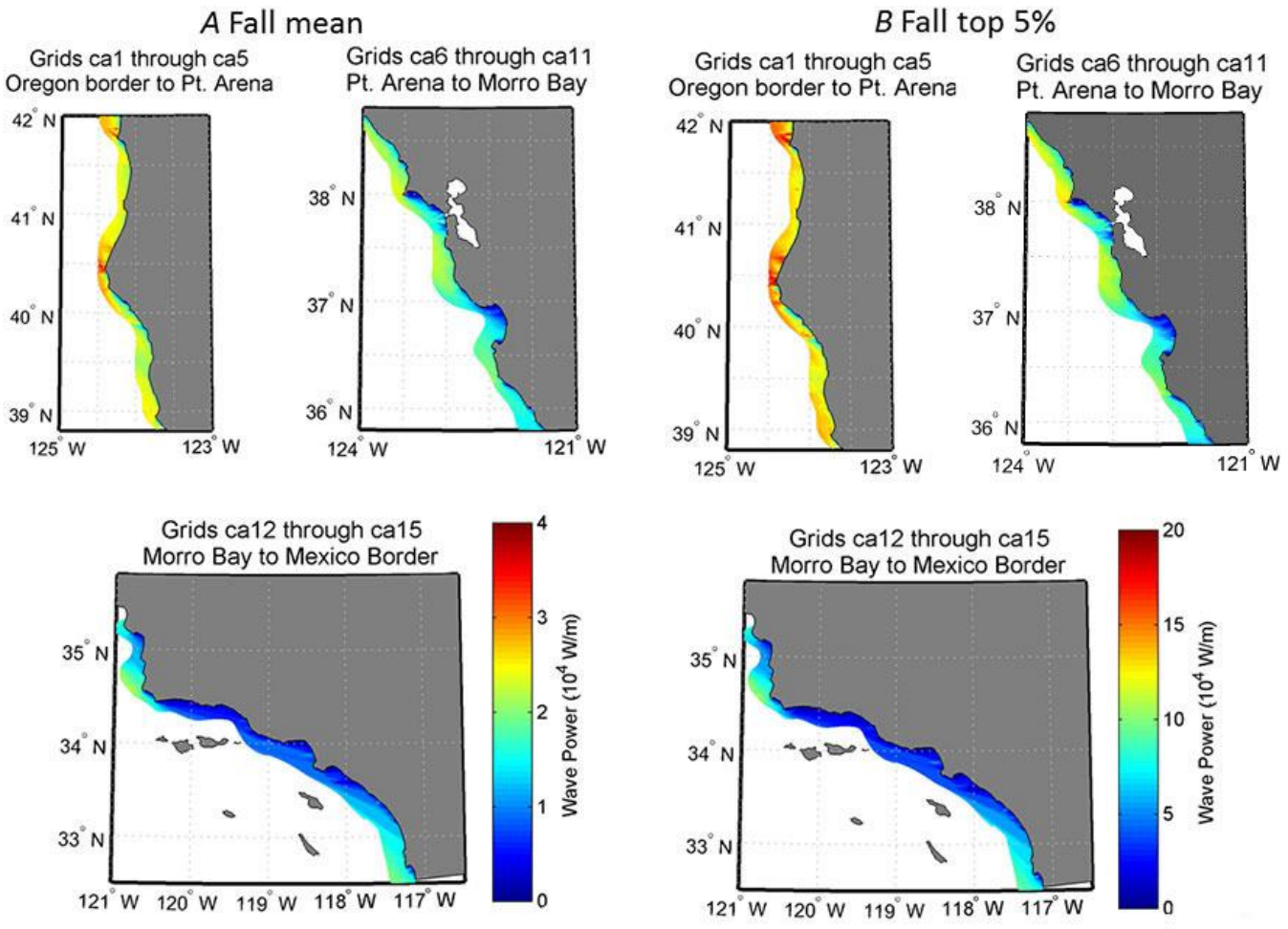

Figure 6. Fall (September-November) wave power along the inner margin of the California shelf. (*A*) Mean and (B) extreme (top 5%) conditions.

Near-bed wave-orbital velocities show similar patterns but are difficult to decipher at the scale offered in figs 3-6. As an alternative, and because this document is intended to provide an overview to the downloadable data rather than detailed analysis, seasonal and latitudinal patterns are evaluated on a per grid basis by obtaining average values at each of the 15 grids (figs. 7 and 8). This type of comparison shows that during extreme winter, spring, and fall conditions, wave power is much greater than average conditions during any other time of the year and extremes during the summer. In fact,

summer extremes are only slightly greater than average spring and fall wave power. Similarly, near-bed wave-orbital velocities during extreme summer conditions are about equal to background spring and fall near bed disturbances. In a general sense, extreme conditions during spring and fall yield very similar near-bed disturbances, with maximum across shelf averaged near-bed wave-orbital velocities reaching approximately 1.1 m/s at the north end of the State.

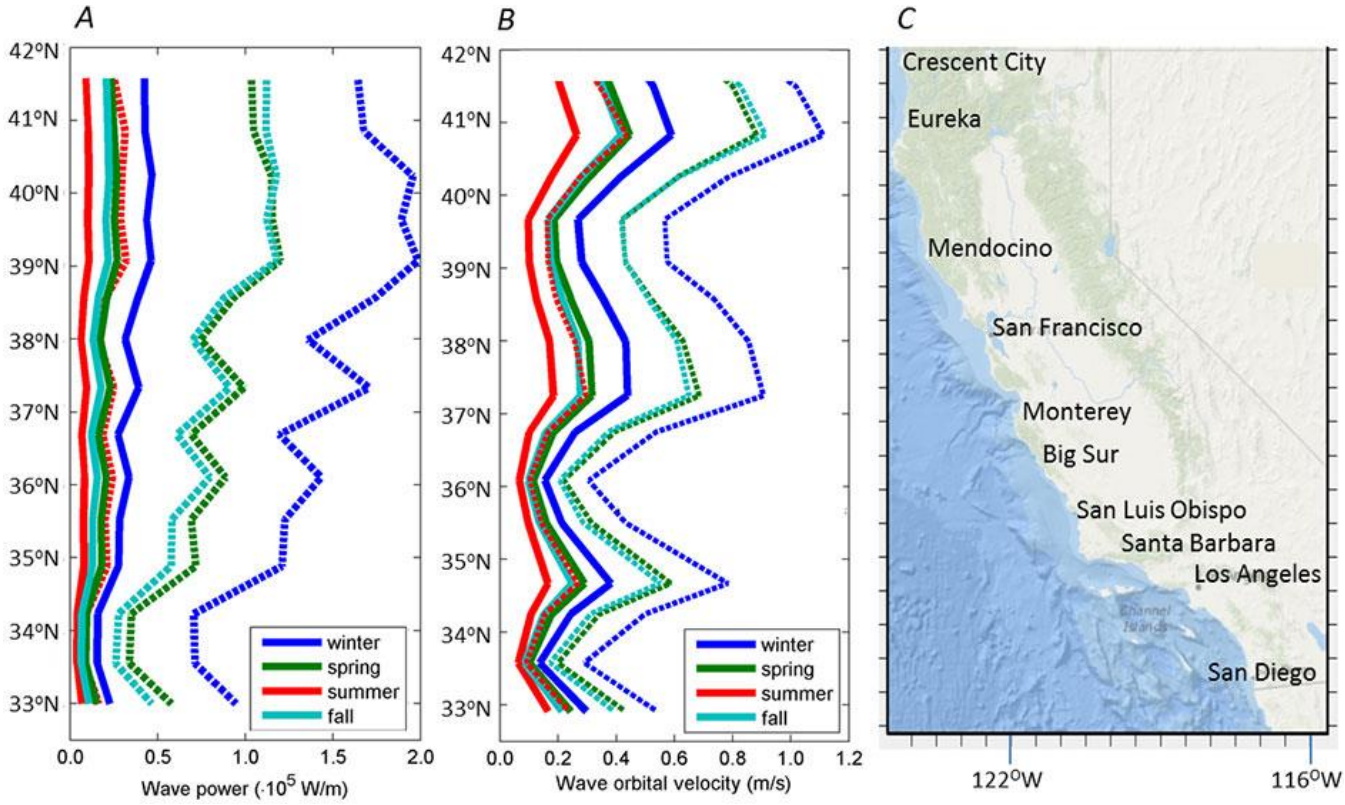

Figure 7. Model grid-averaged wave and seabed energetics as a function of latitude. (*A*) Wave power, and (*B*) wave-orbital velocities. (*C*) Reference map showing locations for *A* and *B*.

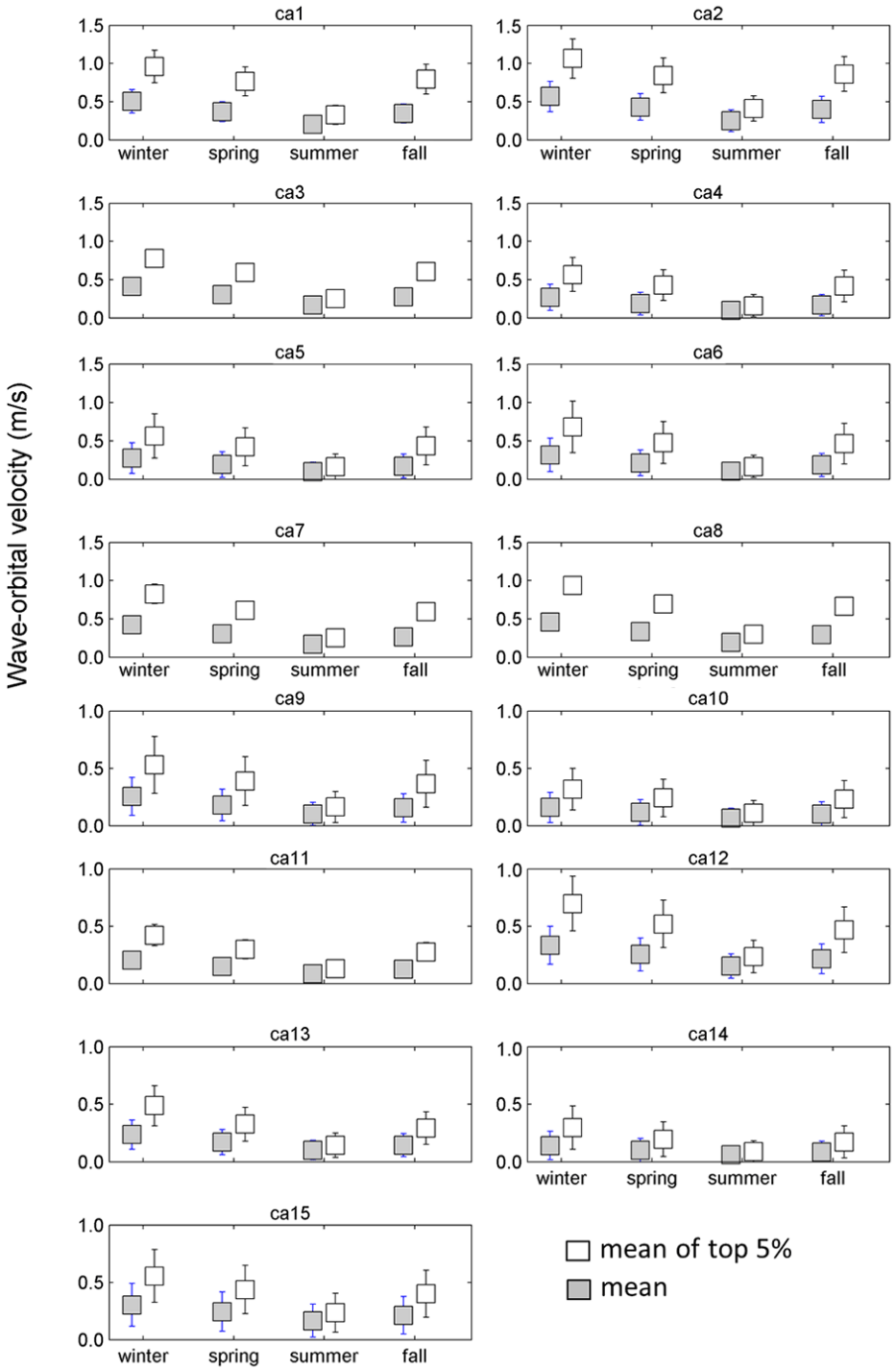

Figure 8. Seabed wave-orbital mean and standard deviation velocities of each grid separated by season for mean (gray squares) and top 5% (white squares) conditions. Note the variation in the scale of the vertical axes varies with latitude.

While these results do not address to what degree these wave motions impact the seabed, they do show that peak wave-induced wave-orbital velocities are more than twice the near-bed tidal current speeds and subtidal current speeds observed along California (for example, Sherwood and others, 1994; Steger and others, 1998; Noble and Ramp, 2000; Storlazzi and Jaffe, 2002, Xu and others, 2002; Storlazzi and others, 2003, Drake and others, 2005), supporting the conclusion that this is a wave-dominated shelf. These results suggest that benthic infauna and epifauna along this continental shelf are adapted to a dynamic hydrodynamic environment. Many of the deeper bedrock reefs are frequently subjected to 0.1-0.2 m/s wave-orbital velocities, and almost all of the shallow bedrock reefs on the inner most portions of the continental shelf (less than 10 m depth, generally less than 1 km from shore), except those in the lee of headlands, are frequently subjected to strong wave-orbital velocities (greater than 0.5 m/s). These shallow bedrock reefs along California typically host giant kelp forests, which are second only to tropical rainforests in biomass production per m^2 (Mann, 1973), and thus the kelp plants and the ecosystem they support have developed in this wave-impacted environment. The spatial and temporal variability in frequency of elevated wave-orbital velocities likely plays into the life history of many organisms and the structure of their ecosystems (for example, species diversity), as suggested by Connell (1978). The community structure of numerous temperate water sessile organisms is influenced by spatial and temporal variations in wave energy similar to those described here. Large wave events have been shown to decrease kelp forest biomass (Graham et al., 1997), increase benthic macroalgae species richness (Wernberg and Goldberg, 2008), and cause mass mortality of nearshore fish species (Bodkin and others, 1987).

References Cited

Allan, J., and Komar, P.D., 2000. Are ocean wave heights increasing in the eastern North Pacific? EOS, Transactions of the American Geophysical Union, 81, 561-567.

Battjes, J., and Janssen, J., 1978. Energy loss and set-up due to breaking of random waves. In Proceedings 16th International Conference Coastal Engineering, ASCE, pp. 569-587.

Bodkin, J.L, VanBlaricom, G.R., and Jameson, R.J., 1987. Mortalities of kelp-forest fishes associated with large oceanic waves off central California: 1982-1983. Environmental Biology of Fishes, 18(1), 73-76.

Booij, N., Ris, R.C., and Holthuijsen, L.H., 1999. A third generation model for coastal regions, Part I – Model description and validation. Journal of Geophysical Research, 104(C4), 7649-7666.

Bromirski, P.D., Cayan, D.R., and Flick, R.E., 2005. Wave spectral energy variability in the Northeast Pacific. Journal of Geophysical Research, 110(C03005), doi:10.1029/2004JC002398.

Coastal and Hydraulics Laboratory, 2013. Wave Information Studies – Pacific data. Engineer Research and Development Center, US Army Corps of Engineers. [http://wis.usace.army.mil/hindcasts.shtml?dmn=pacWIS4]

Connell, J. H., 1978. Diversity in tropical rain forests and coral reefs. Science, 199, 1302–1310.

Demirbilik, Z., and Linwood, V.C. (2002). "Water wave mechanics," In: Coastal Engineering Manual, Part II-1 , Engineer Manual 1110-2-1100, U.S. Army Corps of Engineers, Washington, DC.

Drake, P., McManus, M.A., and Storlazzi, C.D., 2005. Local wind forcing of the Monterey Bay area inner shelf. Continental Shelf Research, 25, 397-417.

Garrison, T. 1996. Oceanography. An Invitation to Marine Science. Second Edition. Wadsworth Publishing Company.

Goodsell, P.J., and Connell, S.D., 2005. Historical configuration of habitat influences and the effects of the disturbance on mobile invertebrates. Marine Ecology Progress Series, 299, 79-87.

Graham, M.H., Harrold, C., Lisin, S., Light, K., Watanabe, J.M., and Foster, M.S., 1997. Population dynamics of giant kelp *Macrocystis pyrifera* along a wave exposure gradient. Marine Ecology Progress Series, 148, 269-279.

Griffen, J.D., Hemer, M.A., and Jones, B.G., 2008. Mobility of sediment grain size distributions on a wave dominated continental shelf, southeastern Australia. Marine Geology, 252, 13-23.

Gunther, H., Hasselmann, S., Janssen, P.A.E.M., 1992 Technical Report No. 4 WAM Model Cycle 4. Technical Report. [http://info.dkrz.de/forschung/reports/report4/wamh-1.html]

Hemer, M.A., 2006. The magnitude and frequency of combined flow bed shear stress as a measure of exposure on the Australian continental shelf. Continental Shelf Research, v. 26, p. 1258-1280.

Inman, D.L. and Jenkins, S.A., 1997. Changing wave climate and littoral drift. California and World Ocean, ’97, Conference Proceedings, chap. 73, 539-549.

Komen, G., Hasselmann, S, and Hasselmann, K., 1984. On the existence of a fully developed

wind-sea spectrum. Journal of Physical Oceanography(14), pp. 1271-1285.

Komen, G.J, Cavaleri, L., Donelan, M., Hasselmann, K., Hasselmann, S. and Janssen, P.A.E.M., 1994. Dynamics and Modeling of Ocean Waves. Cambridge University Press, 532 p.

Mann, K.H., 1973. Seaweeds- their productivity and strategy for growth. Science, 182, 975-981.

National Data Buoy Center, 2006. Station 46042 – MONTEREY data. National Oceanic and Atmospheric Administration. [http://www.ndbc.noaa.gov/station_page.php?station=46042].

Noble, M.A., and Ramp, S.R., 2000. Subtidal currents over the central California slope: Evidence for offshore veering of the undercurrent and for direct, wind-driven slope currents. Deep-Sea Research II, 47, 871-906.

Oceanweather, Inc., 2012. MetOcean data. [http://www.oceanweather.com/metocean/]

Porter-Smith, R., Harris, P.T., Andersen, O.B., Coleman, R., Greensdale, D., and Jenkins, C.J., 2004. Classification of the Australian continental shelf based on predicted sediment threshold exceedance from tidal currents and swell waves. Marine Geology, 211, 1-20.

Ris, R.C., 1997. Spectral modeling of wind waves in coastal areas. Delft, The Netherlands, Ph.D. dissertation, Delft University of Technology, Department of Civil Engineering, Communications on Hydraulic and Geotechnical Engineering, Report No. 97-4.

Ris, R.C., Booij, N., and Holthuijsen, L.H., 1999. A third-generation wave model for coastal regions: Part II –Verification.: Journal of Geophysical Research, 104(C4), 7667-7682.

Roff, J.C., Taylor, M.E., and Laughren, J., 2003. Geo-physical approaches to the classification, delineation, and monitoring of marine habitats and their communities. Aquatic Conservation-Marine and Freshwater Ecosystems, 13, 77-90.

Seymour, R.J., Strange, R.R., Cayan, D.R. and Nathan, R.A., 1984. Influence of El Niños on California's wave climate. Proceedings of the 19th Coastal Engineering Conference, American Society of Civil Engineers, 1, 577-592.

Seymour, R.J., 1998. Effects of El Niños on the West Coast wave climate. Shore and Beach, 66(3), 3-6.

Sherwood, C.R., Butman, B., Cacchione, D.A., Drake, D.E., Gross, T.F., Sternberg, R.W., Wiberg, P.L., and Williams, A.J. III, 1994. Sediment-transport events on the northern California continental shelf during the 1990-1991 STRESS experiment. Continental Shelf Research, 14, 1063-1100.

Snelgrove, P.V.R., and Butman, C.A., 1994. Animal-sediment relationships revisited – Cause versus effect. Oceanography and Marine Biology Annual Review, 32, 111-177.

Steger, J.M., Collins, C.A., Schwing, F.B., Noble, M., Garfield, N., and Steiner, M.T., 1998. An empirical model of the tidal currents in the Gulf of the Farallones. Deep-Sea Research II, 45, 1471-1505.

Storlazzi, C.D. and Griggs, G.B., 2000. The influence of El Niño-Southern Oscillation (ENSO) events on the evolution of central California's shoreline. Geological Society of America Bulletin, 112(2), 236-249.

Storlazzi, C.D., and Jaffe, B.E., 2002. Flow and sediment suspension events on the inner shelf of central California. Marine Geology, 181(1-3), 195-213.

Storlazzi, C.D., McManus, M.A., and Figurski, J.D., 2003. Long-term high-frequency ADCP and temperature measurements along central California: Insights into upwelling and internal waves on the inner shelf. Continental Shelf Research, 23, 901-918.

Storlazzi, C.D., Reid, J.A., 2010. The influence of El Nino-Southern Oscillation (ENSO) cycles on wave-driven sea-floor sediment mobility along the central California continental margin. Continental Shelf Research, 30, 1582-1599.

SWAN team. 2013. SWAN, Scientific and Technical documentation SWAN Cycle III version 70.91ABC, Delft University of Technology, The Netherlands. http://swanmodel.sourceforge.net/online_doc/swantech/swantech.html

Thrush, S.F., and Dayton, P.K., 2002. Disturbance to marine benthic habitats by trawling and dredging-implications for marine biodiversity. Annual Reviews of Ecology and Systematics, 33, 449-473.

Wernberg, T., and Goldberg, N., 2008. Short-term temporal dynamics of algal species in a subtidal kelp bed in relation to changes in environmental conditions and canopy biomass. Estuarine, Coastal and Shelf Science, 76, 265-272.

Xu., J.P., Noble, M., and Eittreim, S. L., 2002. Suspended sediment transport on the continental shelf near Davenport, California. Marine Geology, 181(1-3), 171-194.

Appendix A

Mean and top 5% wave conditions at each WIS station used as boundaries to the SWAN model.

Table A-1. Mean boundary conditions derived from the WIS station data – winter and spring.

WIS ID	Latitude (°N)	Longitude (°W)	Depth (m)	Winter (Dec-Feb)					Spring (Mar-May)				
				H_s (m)	T_p (s)	D_m (º)	U_a (m/s)	U_{dir} (º)	H_s (m)	T_p (s)	D_m (º)	U_a (m/s)	U_{dir} (º)
83037	42.50	124.67	227	3.3	14	272	9	200	2.5	12.0	284	8	309
83038	42.33	124.67	365	3.3	14	272	9	200	2.6	12.0	285	8	311
83039	42.17	124.50	148	3.1	14	273	9	200	2.5	12.0	285	8	312
83040	42.00	124.50	157	3.2	14	273	9	200	2.5	12.0	286	8	314
83041	41.83	124.42	193	3.1	14	274	9	199	2.5	12.0	287	8	316
83042	41.67	124.25	63	2.8	14	271	9	199	2.3	12.0	283	8	317
83043	41.50	124.25	77	3.0	14	275	9	199	2.4	12.0	287	8	319
83044	41.33	124.25	100	3.0	14	277	9	199	2.5	12.0	289	8	320
83045	41.17	124.25	107	3.0	14	279	9	199	2.4	12.0	291	8	322
83046	41.00	124.25	63	2.9	14	281	8	198	2.4	12.0	292	8	324
83047	40.83	124.42	260	3.1	14	281	8	201	2.6	12.0	294	8	323
83048	40.67	124.50	340	3.1	14	281	8	206	2.6	12.0	294	8	324
83049	40.50	124.50	128	3.1	14	280	8	214	2.6	12.0	293	8	324
83050	40.33	124.50	704	3.1	14	281	8	223	2.6	12.0	294	8	324
83051	40.17	124.42	477	3.1	14	281	7	237	2.5	12.0	292	7	324
83052	40.00	124.25	724	3.0	14	279	8	297	2.4	12.0	288	8	324
83053	39.83	124.00	170	2.8	14	277	6	352	2.2	12.0	285	6	322
83054	39.67	124.00	489	3.0	14	281	8	350	2.4	12.0	289	7	323
83055	39.50	124.00	574	3.0	14	282	8	350	2.5	12.0	292	7	323
83056	39.33	124.00	541	3.0	14	283	8	351	2.5	12.0	293	7	323
83057	39.17	123.92	247	3.0	14	283	6	354	2.5	12.0	293	6	323
83058	39.00	123.92	325	3.0	14	284	8	354	2.5	12.0	294	7	323
83059	38.83	123.75	120	2.8	14	280	7	350	2.3	12.0	290	7	323
83060	38.67	123.50	99	2.3	14	272	4	349	1.8	12.0	279	3	321
83061	38.50	123.42	134	2.7	14	279	7	345	2.2	12.0	288	7	322
83062	38.33	123.25	108	2.7	14	280	7	343	2.3	12.0	289	8	323
83063	38.17	123.17	99	2.7	14	282	7	342	2.3	12.0	291	7	323
83064	38.00	123.17	137	2.8	14	283	6	341	2.4	12.0	292	6	323
83065	37.83	122.92	72	2.5	14	280	6	339	2.1	12.0	288	6	324
83066	37.67	122.67	39	2.3	14	271	6	338	1.9	13.0	280	6	324
83067	37.50	122.67	72	2.3	14	277	6	338	2	12.0	286	6	324
83068	37.33	122.67	98	2.6	14	282	7	337	2.3	12.0	291	7	325
83069	37.17	122.67	191	2.7	14	286	7	336	2.4	12.0	295	8	325
83070	37.00	122.50	314	2.7	14	287	7	336	2.4	12.0	295	8	326

83071	36.92	122.25	454	2.4	14	283	7	338	2.1	12.0	289	8	326
83072	36.83	122.00	267	2.0	14	278	5	340	1.7	12.0	282	6	326
83073	36.67	122.17	1435	2.7	14	288	7	339	2.4	12.0	295	8	326
83074	36.50	122.17	1353	2.8	14	290	7	340	2.5	12.0	297	8	327
83075	36.33	122.00	203	2.7	14	290	7	341	2.4	12.0	297	8	327
83076	36.17	121.92	971	2.7	14	290	5	342	2.4	12.0	296	6	327
83077	36.00	121.75	1037	2.7	14	290	6	342	2.4	12.0	295	8	327
83078	35.83	121.67	849	2.7	14	291	6	342	2.4	12.0	296	7	327
83079	35.67	121.50	651	2.7	14	291	6	342	2.4	12.0	296	7	327
83080	35.50	121.25	434	2.6	14	289	6	342	2.3	13.0	294	7	327
83081	35.33	121.17	463	2.6	14	291	6	341	2.4	12.0	296	7	327
83082	35.17	121.00	399	2.6	14	291	6	340	2.3	13.0	296	8	326
83083	35.00	120.75	94	2.3	14	288	7	338	2.1	12.0	293	8	325
83084	34.83	120.92	313	2.6	14	293	7	338	2.4	12.0	299	8	325
83085	34.67	120.92	433	2.7	14	294	7	336	2.5	12.0	300	8	324
83086	34.50	120.75	438	2.6	14	294	7	331	2.5	12.0	300	8	321
83087	34.42	120.58	302	2.4	14	290	4	330	2.1	12.0	295	5	320
83088	34.33	120.42	363	2.1	14	288	5	325	1.9	12.0	291	6	315
83090	34.25	120.00	569	1.5	14	282	5	324	1.3	12.0	284	7	308
83091	34.25	119.75	301	1.1	13	278	5	330	1	11.0	279	6	306
83092	34.25	119.50	109	0.9	13	273	5	337	0.8	11.0	272	6	304
83093	34.17	119.42	160	1.0	13	279	4	331	0.9	12.0	278	5	300
83096	33.92	119.17	771	0.8	13	261	5	324	0.9	13.0	255	6	286
83099	33.83	118.67	802	0.9	13	263	5	326	1	13.0	255	5	272
83100	33.67	118.50	783	0.9	13	271	5	320	1	12.0	267	5	273
83101	33.58	118.25	534	0.9	13	272	4	316	0.9	11.0	268	4	279
83102	33.50	118.00	467	0.8	14	268	4	315	0.9	13.0	259	5	273
83103	33.33	117.92	672	0.7	13	258	4	313	0.8	13.0	250	5	280
83105	33.08	117.67	824	1.0	14	269	4	315	1	13.0	261	5	285
83107	32.75	117.50	848	1.1	14	276	5	317	1.2	13.0	269	5	293
Minimum			39	0.7	13	258	4	198	0.8	11	250	3	272
Maximum			1435	3.3	14	294	9	354	2.6	13	300	8	327
Mean			395	2.4	14	280	7	305	2.1	12	287	7	316
Standard Deviation			318	0.8	0.3	8	2	57	0.6	0.4	12	1	15

Table A-2. Mean boundary s conditions derived from WIS station data – summer and fall.

WIS ID	Latitude (°N)	Longitude (°W)	Depth (m)	Summer (Jun-Aug)					Fall (Sep-Nov)				
				H_s (m)	T_p (s)	D_m (º)	U_a (m/s)	U_{dir} (º)	H_s (m)	T_p (s)	D_m (º)	U_a (m/s)	U_{dir} (º)
83037	42.50	124.67	227	1.8	9	306	8	342	3	12	290	7	328
83038	42.33	124.67	365	1.8	10	308	8	341	3	12	291	7	329
83039	42.17	124.50	148	1.8	9	306	8	341	2	12	291	7	331
83040	42.00	124.50	157	1.8	9	307	8	341	2	12	292	7	332
83041	41.83	124.42	193	1.8	9	307	8	341	2	12	292	7	333
83042	41.67	124.25	63	1.6	9	302	8	341	2	12	288	7	334
83043	41.50	124.25	77	1.8	9	306	8	340	2	12	292	7	335
83044	41.33	124.25	100	1.9	9	309	8	340	2	12	294	7	336
83045	41.17	124.25	107	1.9	9	310	8	340	2	12	296	7	337
83046	41.00	124.25	63	1.9	9	312	8	340	2	12	298	7	338
83047	40.83	124.42	260	2.0	9	314	8	339	2	12	299	7	338
83048	40.67	124.50	340	2.0	9	314	8	338	2	12	299	7	337
83049	40.50	124.50	128	2.0	9	313	8	337	2	12	298	7	337
83050	40.33	124.50	704	2.0	9	311	8	336	2	12	299	7	337
83051	40.17	124.42	477	1.9	10	306	6	335	2	12	297	6	337
83052	40.00	124.25	724	1.7	10	298	7	333	2	12	293	7	336
83053	39.83	124.00	170	1.5	10	291	5	330	2	12	289	5	335
83054	39.67	124.00	489	1.7	10	298	7	330	2	12	294	6	335
83055	39.50	124.00	574	1.8	10	301	7	330	2	12	296	6	335
83056	39.33	124.00	541	1.8	10	303	7	329	2	12	297	6	335
83057	39.17	123.92	247	1.8	10	303	5	329	2	12	297	5	335
83058	39.00	123.92	325	1.9	10	304	6	328	2	12	298	6	334
83059	38.83	123.75	120	1.7	10	299	6	327	2	12	294	6	334
83060	38.67	123.50	99	1.2	11	280	3	326	2	12	281	3	333
83061	38.50	123.42	134	1.5	10	292	6	325	2	12	291	6	332
83062	38.33	123.25	108	1.6	10	293	6	325	2	12	292	6	332
83063	38.17	123.17	99	1.6	10	296	6	325	2	12	294	6	332
83064	38.00	123.17	137	1.7	10	298	5	325	2	12	296	5	332
83065	37.83	122.92	72	1.5	10	292	5	324	2	12	291	5	332
83066	37.67	122.67	39	1.3	11	285	5	324		13	282	5	332
83067	37.50	122.67	72	1.5	10	291	5	324	2	12	288	5	332
83068	37.33	122.67	98	1.7	10	295	6	324	2	12	293	6	332
83069	37.17	122.67	191	1.8	10	298	7	324	2	12	297	6	332
83070	37.00	122.50	314	1.8	10	298	7	324	2	12	297	7	332
83071	36.92	122.25	454	1.6	10	290	7	324	2	12	290	6	332
83072	36.83	122.00	267	1.2	11	279	5	323	1	13	282	5	332
83073	36.67	122.17	1435	1.7	10	296	7	324	2	12	297	6	332

83074	36.50	122.17	1353	1.8	10	298	7	323	2	12	299	6	332
83075	36.33	122.00	203	1.8	10	298	7	323	2	12		6	332
83076	36.17	121.92	971	1.7	10	296	5	323	2	12	298	5	332
83077	36.00	121.75	1037	1.7	10	294	6	322	2	12	297	6	332
83078	35.83	121.67	849	1.7	10	296	6	322	2	12	298	5	332
83079	35.67	121.50	651	1.7	10	295	6	322	2	12	298	6	332
83080	35.50	121.25	434	1.6	11	291	6	322	2	13	295	6	332
83081	35.33	121.17	463	1.7	10	294	6	322	2	12	297	5	332
83082	35.17	121.00	399	1.6	10	294	6	322	2	12	297	6	331
83083	35.00	120.75	94	1.5	10	292	7	321	2	12	294	6	330
83084	34.83	120.92	313	1.7	10	298	7	321	2	12	300	6	330
83085	34.67	120.92	433	1.8	10		7	321	2	12	301	6	329
83086	34.50	120.75	438	1.8	10	299	7	318	2	12	301	6	326
83087	34.42	120.58	302	1.5	10	292	4	317	2	12	295	4	324
83088	34.33	120.42	363	1.3	11	288	5	312	2	13	292	5	320
83090	34.25	120.00	569	0.8	10	279	6	303	1	12	283	5	314
83091	34.25	119.75	301	0.6	9	277	5	300	1	11	279	5	315
83092	34.25	119.50	109	0.6	11	252	4	297		12	261	4	316
83093	34.17	119.42	160	0.6	11	260	4	294	1	12	269	4	312
83096	33.92	119.17	771	0.8	13	224	5	279	1	13	234	4	301
83099	33.83	118.67	802	0.8	14	234	4	264	1	14	241	4	295
83100	33.67	118.50	783	0.7	13	254	4	266	1	13	259	4	292
83101	33.58	118.25	534	0.6	11	235	3	274	1	12	249	3	295
83102	33.50	118.00	467	0.7	13	221	4	269	1	13	234	4	291
83103	33.33	117.92	672	0.7	14	212	4	276	1	14	223	4	294
83105	33.08	117.67	824	0.8	14	227	4	282	1	14	238	4	298
83107	32.75	117.50	848	0.9	13	237	4	290	1	14	250	4	303
Minimum			39	0.6	9	212	3	264	0.6	11	223	3	291
Maximum			1435	2.0	14	314	8	342	2.5	14	301	7	338
Mean			395	1.5	10	288	6	320	1.8	12	286	6	327
Standard Deviation			318	0.4	1.3	25	1	20	0.6	0.6	19	1	13

Table A-3. Top 5% boundary conditions derived from WIS station data – winter and spring.

WIS ID	Latitude (°N)	Longitude (°W)	Depth (m)	Winter (Dec-Feb)					Spring (Mar-May)				
				H_s (m)	T_p (s)	D_m (°)	U_a (m/s)	U_{dir} (°)	H_s (m)	T_p (s)	D_m (°)	U_a (m/s)	U_{dir} (°)
83037	42.50	124.67	227	6.3	15	258	13	217	5.1	14.0	273	11	248
83038	42.33	124.67	365	6.3	15	259	13	217	5.1	14.0	274	11	252
83039	42.17	124.50	148	6.1	15	260	13	219	4.9	14.0	274	11	255
83040	42.00	124.50	157	6.1	15	261	13	219	5	14.0	276	11	259
83041	41.83	124.42	193	6.0	15	263	13	221	4.9	14.0	277	11	264
83042	41.67	124.25	63	5.5	15	260	12	219	4.5	14.0	272	11	258
83043	41.50	124.25	77	5.7	15	265	12	226	4.7	14.0	279	11	277
83044	41.33	124.25	100	5.7	15	268	12	232	4.8	14.0	283	11	290
83045	41.17	124.25	107	5.7	15	272	12	235	4.7	14.0	287	11	299
83046	41.00	124.25	63	5.5	15	276	12	243	4.7	14.0	290	12	309
83047	40.83	124.42	260	5.9	15	274	12	242	5	14.0	292	12	312
83048	40.67	124.50	340	6.0	15	272	12	242	5	14.0	293	12	314
83049	40.50	124.50	128	5.9	15	270	12	243	5	14.0	291	12	315
83050	40.33	124.50	704	6.1	15	272	12	243	5	14.0	292	12	315
83051	40.17	124.42	477	6.0	15	271	9	241	4.9	14.0	288	9	306
83052	40.00	124.25	724	5.9	15	269	11	236	4.8	14.0	282	10	297
83053	39.83	124.00	170	5.5	15	267	8	233	4.5	14.0	278	7	288
83054	39.67	124.00	489	5.8	15	272	11	241	4.8	14.0	286	11	305
83055	39.50	124.00	574	5.9	15	273	11	246	4.9	14.0	289	11	310
83056	39.33	124.00	541	5.9	15	274	11	248	4.9	14.0	291	11	314
83057	39.17	123.92	247	5.8	15	275	9	249	4.8	14.0	291	9	312
83058	39.00	123.92	325	5.8	15	275	11	250	4.9	14.0	292	11	316
83059	38.83	123.75	120	5.4	15	269	11	245	4.5	14.0	286	11	312
83060	38.67	123.50	99	4.8	15	260	5	227	3.7	14.0	270	5	280
83061	38.50	123.42	134	5.3	15	269	11	244	4.3	14.0	282	11	307
83062	38.33	123.25	108	5.3	15	271	10	252	4.4	14.0	284	11	314
83063	38.17	123.17	99	5.2	15	274	10	261	4.4	14.0	288	11	318
83064	38.00	123.17	137	5.5	16	276	8	265	4.7	14.0	290	8	319
83065	37.83	122.92	72	4.8	15	273	8	261	4	14.0	283	8	314
83066	37.67	122.67	39	4.5	15	262	8	262	3.7	14.0	275	8	316
83067	37.50	122.67	72	4.5	15	266	8	267	3.8	13.0	281	9	320
83068	37.33	122.67	98	5.0	15	274	10	279	4.3	14.0	289	11	325
83069	37.17	122.67	191	5.3	15	280	11	289	4.6	14.0	295	12	328
83070	37.00	122.50	314	5.3	15	280	11	293	4.6	14.0	295	12	329
83071	36.92	122.25	454	4.8	15	274	10	287	4	13.0	287	12	324
83072	36.83	122.00	267	4.2	15	269	7	274	3.4	14.0	277	8	314
83073	36.67	122.17	1435	5.3	15	283	10	298	4.6	14.0	295	12	327
83074	36.50	122.17	1353	5.4	15	285	10	301	4.7	14.0	298	12	327

83075	36.33	122.00	203	5.2	15	285	10	304	4.6	14.0	298	12	327
83076	36.17	121.92	971	5.3	15	285	8	303	4.6	14.0	296	9	326
83077	36.00	121.75	1037	5.2	16	285	9	303	4.5	14.0	295	11	326
83078	35.83	121.67	849	5.3	16	286	9	306	4.6	14.0	297	10	326
83079	35.67	121.50	651	5.2	16	286	9	307	4.5	14.0	297	11	326
83080	35.50	121.25	434	5.0	16	284	9	304	4.3	14.0	294	11	326
83081	35.33	121.17	463	5.1	16	287	9	308	4.5	14.0	296	10	326
83082	35.17	121.00	399	5.1	16	287	10	310	4.4	14.0	297	12	327
83083	35.00	120.75	94	4.6	15	283	10	308	4	14.0	292	12	324
83084	34.83	120.92	313	5.2	15	290	10	313	4.6	14.0	300	12	326
83085	34.67	120.92	433	5.2	15	292	10	315	4.7	14.0	302	12	326
83086	34.50	120.75	438	5.2	15	292	10	313	4.6	14.0	302	12	322
83087	34.42	120.58	302	4.6	15	286	6	310	4	14.0	293	7	318
83088	34.33	120.42	363	4.2	15	282	7	304	3.5	14.0	288	8	313
83090	34.25	120.00	569	3.3	15	278	8	299	2.7	13.0	282	11	306
83091	34.25	119.75	301	2.7	15	275	8	298	2.2	12.0	278	10	303
83092	34.25	119.50	109	2.2	14	271	8	297	1.9	10.0	275	10	299
83093	34.17	119.42	160	2.3	14	278	7	301	2	12.0	280	9	299
83096	33.92	119.17	771	2.2	11	252	9	273	2	8.0	265	11	280
83099	33.83	118.67	802	2.4	11	259	8	276	2.2	9.0	262	10	268
83100	33.67	118.50	783	2.5	12	269	9	282	2.3	9.0	271	10	270
83101	33.58	118.25	534	2.2	13	271	6	283	2	9.0	273	8	276
83102	33.50	118.00	467	2.1	12	266	8	274	1.9	10.0	270	9	270
83103	33.33	117.92	672	2.0	10	257	9	271	1.9	9.0	267	9	276
83105	33.08	117.67	824	2.5	12	267	9	279	2.3	9.0	274	9	282
83107	32.75	117.50	848	2.8	12	271	9	286	2.6	10.0	277	10	291
Minimum			39	2.0	10	252	5	217	1.9	8	262	5	248
Maximum			1435	6.3	16	292	13	315	5.1	14	302	12	329
Mean			395	4.8	15	273	10	269	4.1	13	285	10	304
Standard Deviation			318	1.3	1.3	9	2	31	1.0	1.7	10	2	23

Table A-4. Top 5% boundary conditions derived from WIS station data – summer and fall.

WIS ID	Latitude (°N)	Longitude (°W)	Depth (m)	Summer (Jun-Aug)					Fall (Sep-Nov)				
				H_s (m)	T_p (s)	D_m (°)	U_a (m/s)	U_{dir} (°)	H_s (m)	T_p (s)	D_m (°)	U_a (m/s)	U_{dir} (°)
83037	42.50	124.67	227	3.2	10	316	13	349	5	14	276	11	244
83038	42.33	124.67	365	3.3	10	319	13	350	5	14	277	11	247
83039	42.17	124.50	148	3.2	10	314	13	349	5	14	277	11	249
83040	42.00	124.50	157	3.3	10	317	14	349	5	14	279	11	252
83041	41.83	124.42	193	3.3	10	317	14	349	5	14	280	11	257
83042	41.67	124.25	63	2.8	10	307	14	347	5	14	274	11	251
83043	41.50	124.25	77	3.2	10	315	14	349	5	14	280	11	265
83044	41.33	124.25	100	3.4	10	318	14	349	5	14	283	10	275
83045	41.17	124.25	107	3.4	9	320	14	349	5	14	287	10	284
83046	41.00	124.25	63	3.5	9	322	15	349	5	14	289	10	294
83047	40.83	124.42	260	3.7	10	326	14	349	5	14	292	10	300
83048	40.67	124.50	340	3.8	10	328	14	348	5	14	293	11	303
83049	40.50	124.50	128	3.7	10	326	14	347	5	14	291	10	304
83050	40.33	124.50	704	3.7	10	325	14	346	5	14	293	10	305
83051	40.17	124.42	477	3.4	10	317	11	344	5	14	291	8	300
83052	40.00	124.25	724	3.0	10	305	12	340	5	15	287	9	290
83053	39.83	124.00	170	2.6	11	296	8	336	4	15	283	6	286
83054	39.67	124.00	489	3.0	10	306	11	337	5	15	290	9	300
83055	39.50	124.00	574	3.2	10	310	11	338	5	14	293	9	308
83056	39.33	124.00	541	3.3	10	313	11	338	5	14	295	9	311
83057	39.17	123.92	247	3.2	10	311	9	337	5	14	295	8	313
83058	39.00	123.92	325	3.3	10	313	11	337	5	14	296	9	314
83059	38.83	123.75	120	3.0	10	308	11	336	4	14	290	9	312
83060	38.67	123.50	99	2.0	11	289	5	333	4	14	276	4	293
83061	38.50	123.42	134	2.7	11	300	11	334	4	14	287	9	309
83062	38.33	123.25	108	2.8	10	301	11	334	4	14	289	9	315
83063	38.17	123.17	99	2.9	10	303	10	334	4	14	292	9	321
83064	38.00	123.17	137	3.0	10	306	8	335	5	14	294	7	324
83065	37.83	122.92	72	2.5	11	298	8	334	4	15	288	7	320
83066	37.67	122.67	39	2.3	11	293	9	334	4	15	278	7	322
83067	37.50	122.67	72	2.6	10	300	9	334	3	13	286	8	326
83068	37.33	122.67	98	2.9	10	304	11	334	4	14	293	9	329
83069	37.17	122.67	191	3.2	10	308	12	335	4	14	298	10	332
83070	37.00	122.50	314	3.2	10	307	12	334	4	14	298	10	332
83071	36.92	122.25	454	2.7	10	299	12	332	4	14	291	10	329
83072	36.83	122.00	267	2.1	10	289	8	330	3	14	282	7	323
83073	36.67	122.17	1435	3.1	10	305	11	331	4	14	298	10	332
83074	36.50	122.17	1353	3.2	10	307	11	331	4	14	301	10	332

83075	36.33	122.00	203	3.1	10	306	11	329	4	14	301	10	332
83076	36.17	121.92	971	3.0	10	305	8	329	4	14	301	8	332
83077	36.00	121.75	1037	2.9	10	303	10	328	4	15	300	9	332
83078	35.83	121.67	849	3.0	10	304	9	328	4	14	301	9	333
83079	35.67	121.50	651	3.0	10	304	10	328	4	15	301	9	333
83080	35.50	121.25	434	2.7	11	300	10	328	4	15	298	9	333
83081	35.33	121.17	463	2.9	11	302	9	328	4	15	301	9	333
83082	35.17	121.00	399	2.8	11	302	10	328	4	14	301	10	333
83083	35.00	120.75	94	2.5	10	299	11	327	4	14	296	10	331
83084	34.83	120.92	313	3.0	10	306	10	327	4	14	304	10	333
83085	34.67	120.92	433	3.0	10	308	11	327	4	14	306	10	332
83086	34.50	120.75	438	3.0	10	307	11	324	4	14	305	10	329
83087	34.42	120.58	302	2.5	10	300	7	322	4	14	298	6	327
83088	34.33	120.42	363	2.1	10	295	8	317	3	14	294	7	323
83090	34.25	120.00	569	1.6	9	286	10	309	2	13	286	9	317
83091	34.25	119.75	301	1.3	8	281	9	306	2	12	282	9	317
83092	34.25	119.50	109	1.1	8	275	8	303	1	11	278	8	315
83093	34.17	119.42	160	1.2	9	280	7	300	2	11	283	7	314
83096	33.92	119.17	771	1.3	9	255	9	280	2	10	267	9	299
83099	33.83	118.67	802	1.4	10	256	7	265	2	10	265	8	295
83100	33.67	118.50	783	1.4	7	270	7	268	2	9	275	8	294
83101	33.58	118.25	534	1.2	8	265	5	275	2	9	272	6	296
83102	33.50	118.00	467	1.2	11	251	6	269	1	11	266	7	290
83103	33.33	117.92	672	1.2	12	239	6	277	1	11	259	7	291
83105	33.08	117.67	824	1.4	12	259	6	284	2	11	272	8	298
83107	32.75	117.50	848	1.5	11	269	7	294	2	11	279	8	305
Minimum			39	1.1	7	239	5	265	1.4	9	259	4	244
Maximum			1435	3.8	12	328	15	350	5.4	15	306	11	333
Mean			395	2.7	10	300	10	327	3.9	14	288	9	307
Standard Deviation			318	0.8	0.8	19	3	22	1.2	1.5	11	1	25

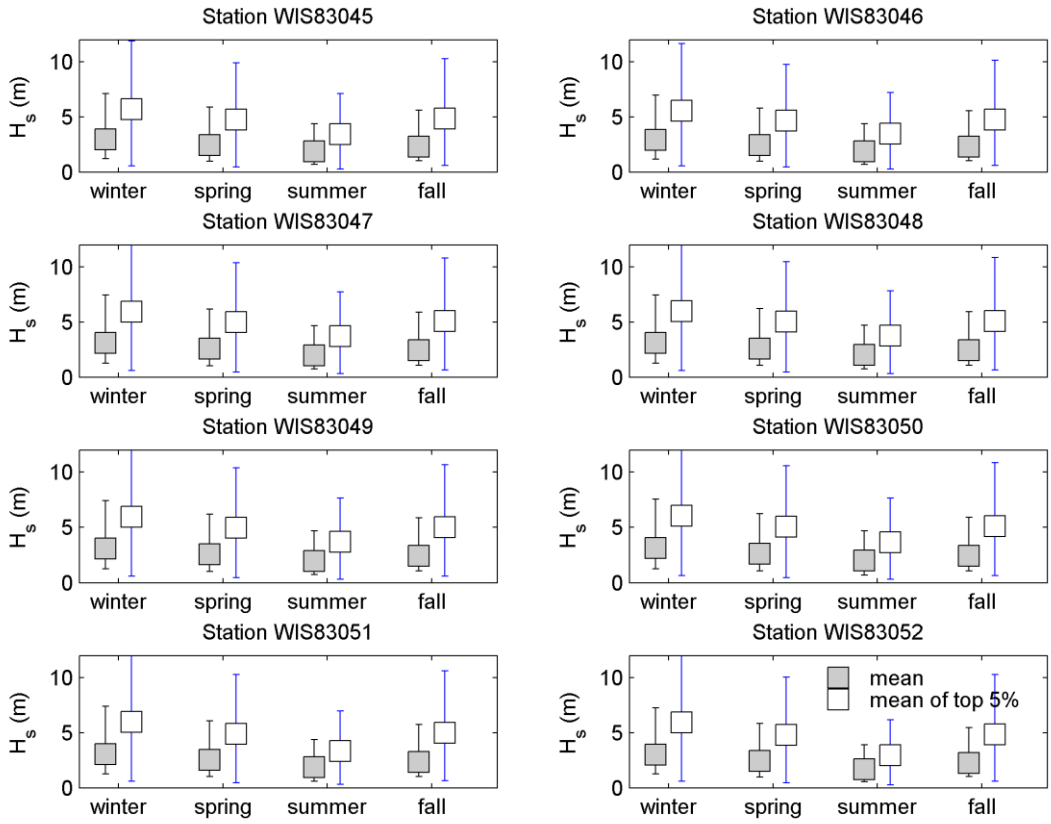

Figure A-1. Mean and extreme (top 5%) wave heights at each WIS station used as boundaries to the SWAN model. Standard deviations are shown with the vertical bars.

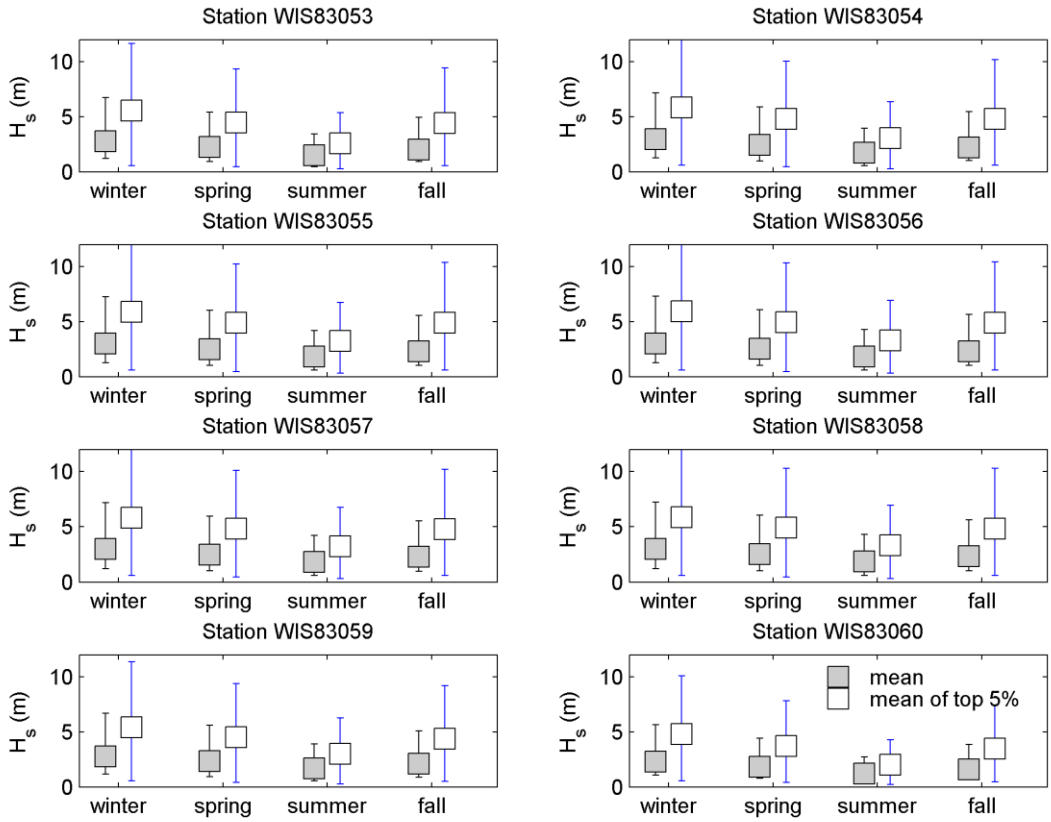

Figure A-2. Mean and extreme (top 5%) wave heights at each WIS station used as boundaries to the SWAN model. Standard deviations are shown with the vertical bars.

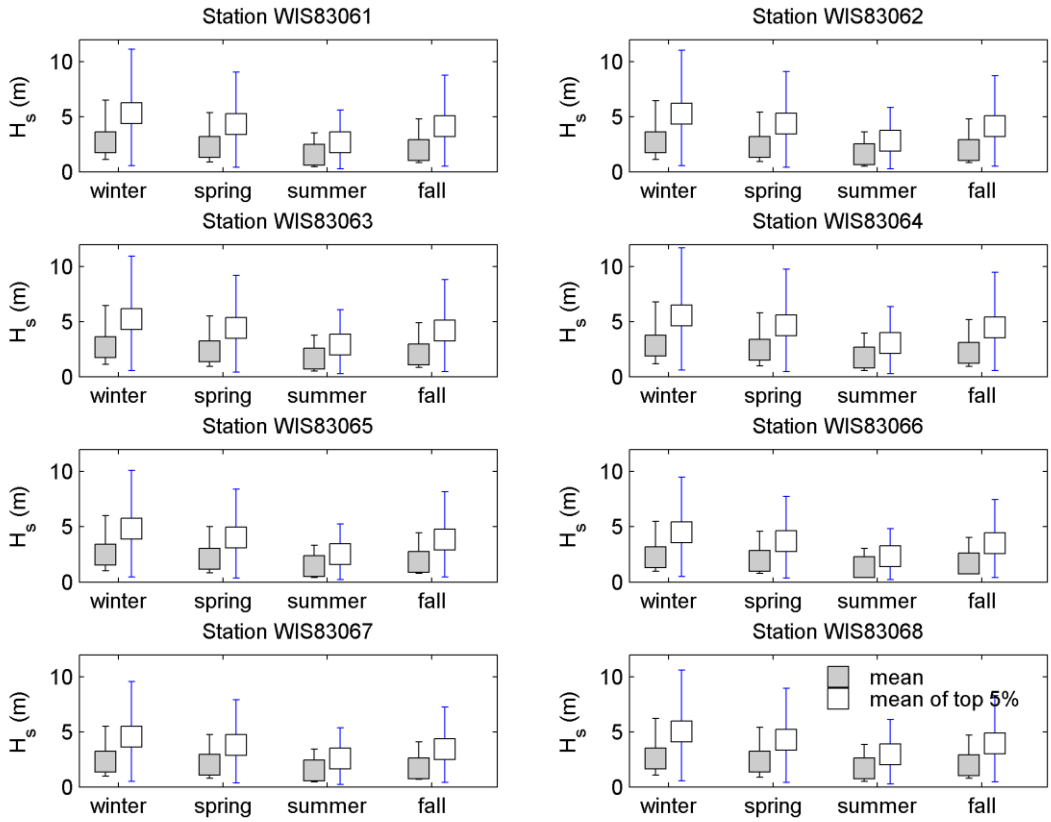

Figure A-3. Mean and extreme (top 5%) wave heights at each WIS station used as boundaries to the SWAN model. Standard deviations are shown with the vertical bars.

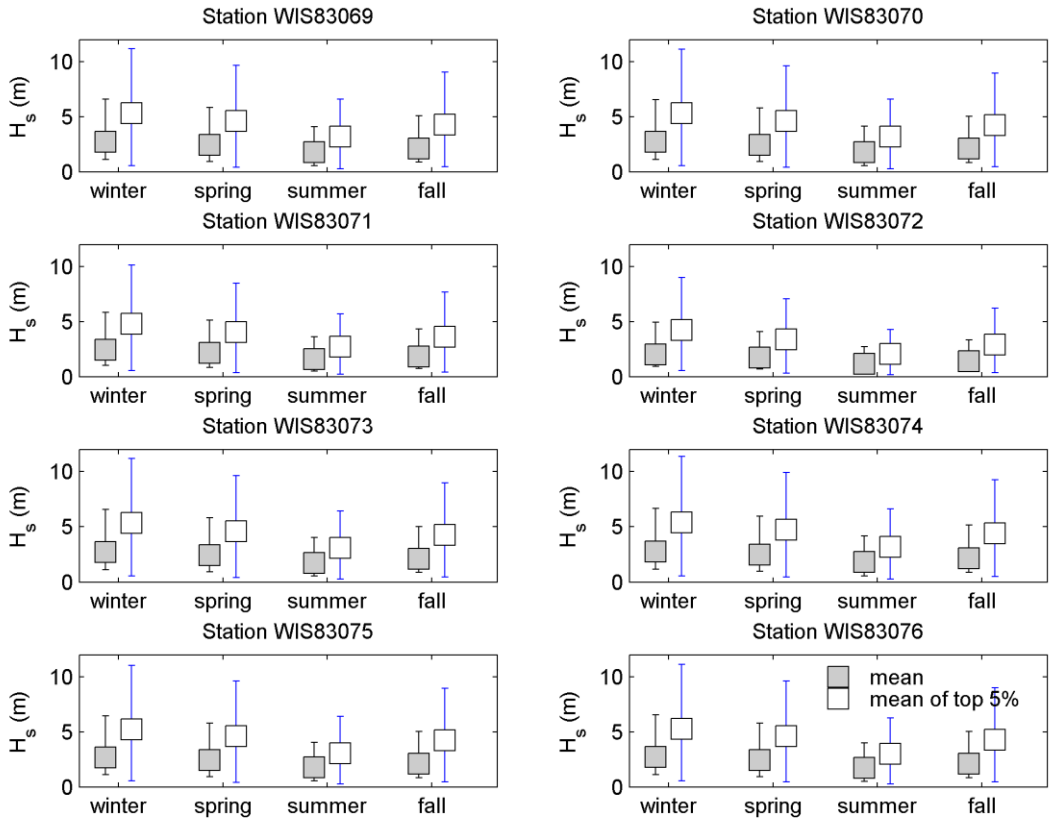

Figure A-4. Mean and extreme (top 5%) wave heights at each WIS station used as boundaries to the SWAN model. Standard deviations are shown with the vertical bars.

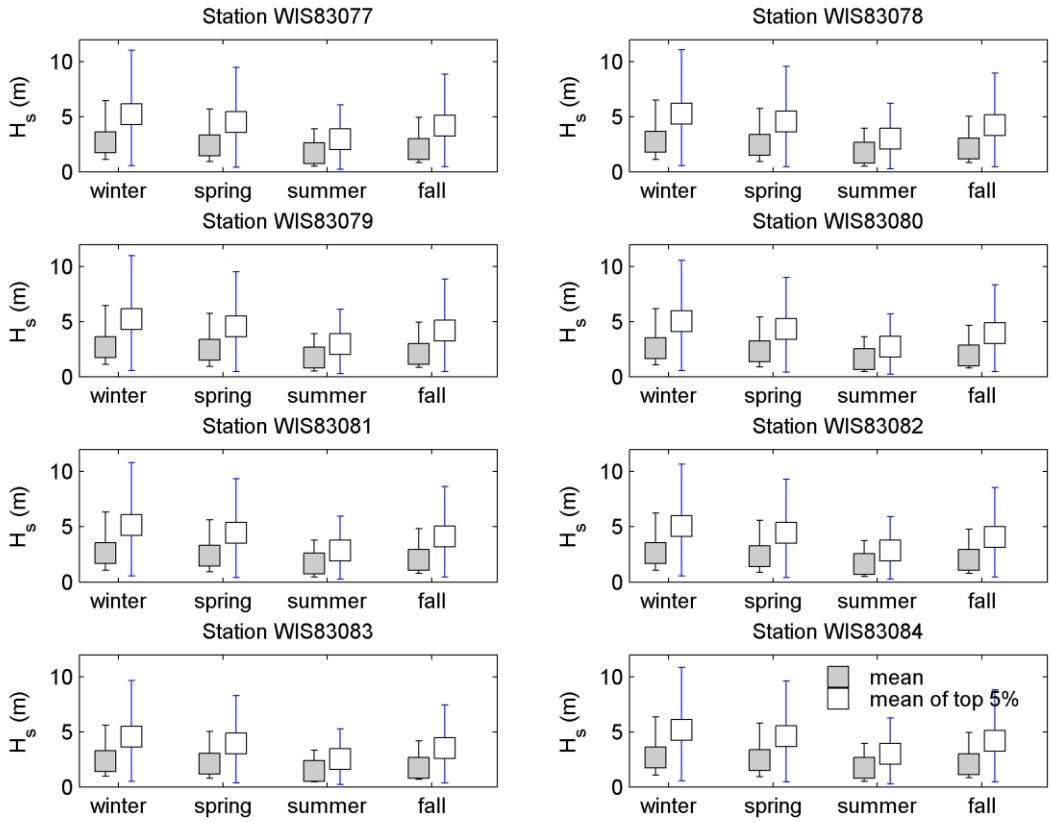

Figure A-5. Mean and extreme (top 5%) wave heights at each WIS station used as boundaries to the SWAN model. Standard deviations are shown with the vertical bars.

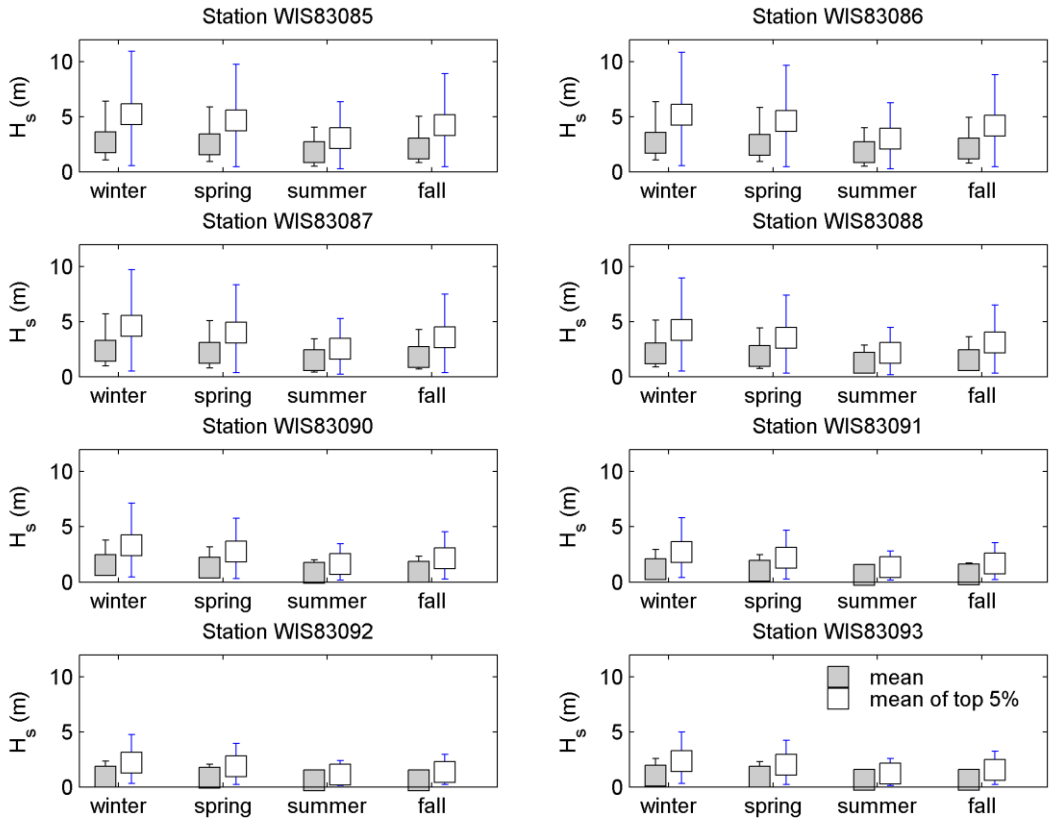

Figure A-6. Mean and extreme (top 5%) wave heights at each WIS station used as boundaries to the SWAN model. Standard deviations are shown with the vertical bars.

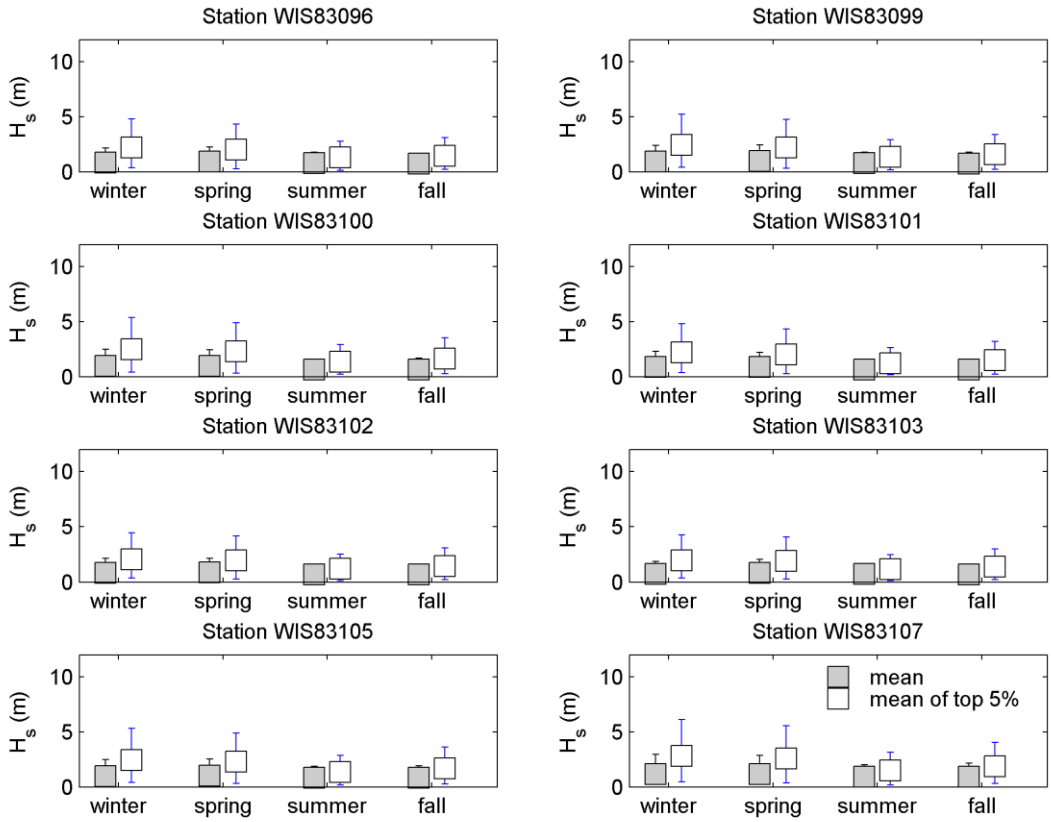

Figure A-7. Mean and extreme (top 5%) wave heights at each WIS station used as boundaries to the SWAN model. Standard deviations are shown with the vertical bars.